iScience

CellPress
OPEN ACCESS

Article

Synthetic carbohydrate-binding agents neutralize SARS-CoV-2 by inhibiting binding of the spike protein to ACE2

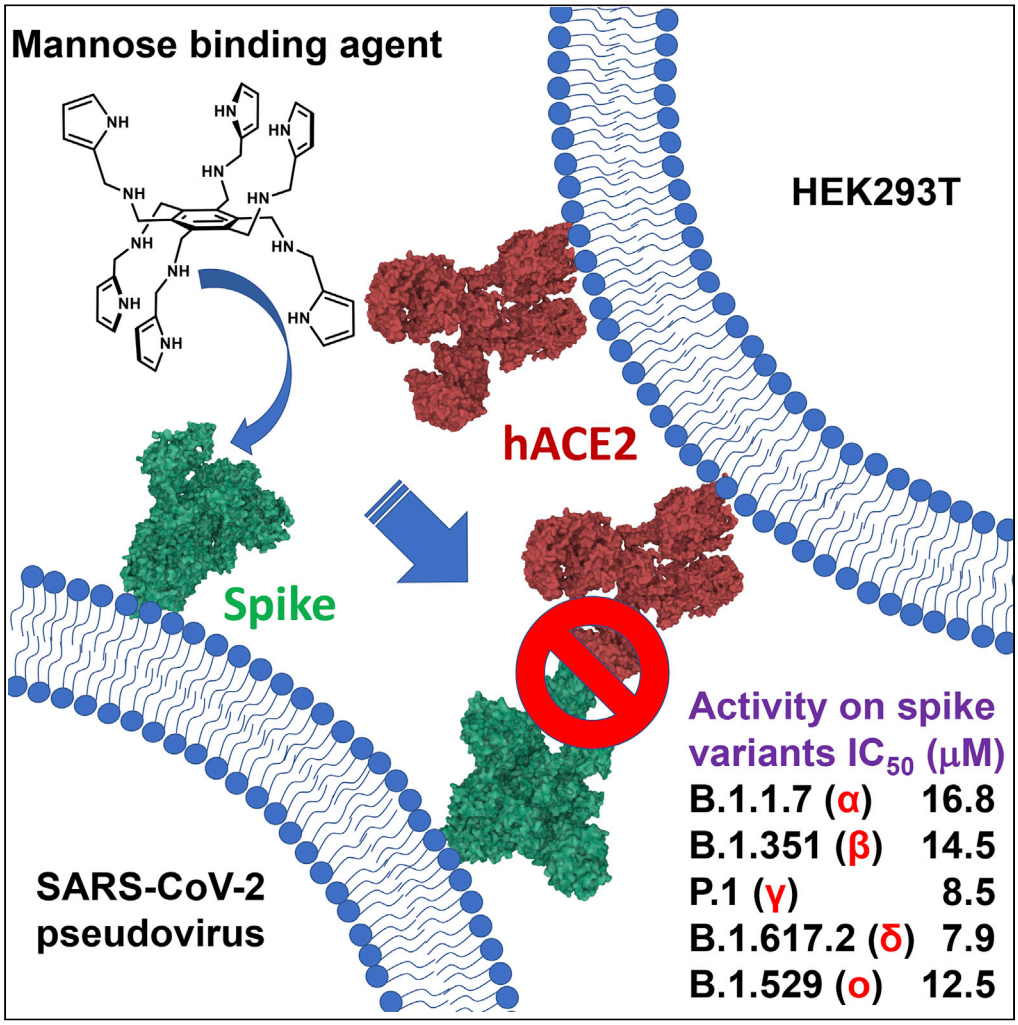

Oscar Francesconi, Lorena Donnici, Marco Fragai, ..., Raffaele De Francesco, Cristina Nativi, Stefano Roelens

grifantini@ingm.org (R.G.)
defrancesco@ingm.org (R.D.F.)
cristina.nativi@unifi.it (C.N.)

Highlights

Mannose-binding CBAs inhibit SARS-CoV-2 infection showing broad neutralizing activity

CBAs interact with the spike protein rather than with ACE2 receptors

The non-toxic CBA IDS060 binds to the spike RBD and inhibits binding of RBD to hACE2

Francesconi et al., iScience 25, 104239
May 20, 2022
https://doi.org/10.1016/j.isci.2022.104239

iScience

CellPress
OPEN ACCESS

Article

Synthetic carbohydrate-binding agents neutralize SARS-CoV-2 by inhibiting binding of the spike protein to ACE2

Oscar Francesconi,[1,6] Lorena Donnici,[2,6] Marco Fragai,[1,3,7] Elisa Pesce,[2] Mauro Bombaci,[2] Alessandra Fasciani,[2] Lara Manganaro,[2,4] Matteo Conti,[2] Renata Grifantini,[2,*] Raffaele De Francesco,[2,4,*] Cristina Nativi,[1,7,*] and Stefano Roelens[5]

SUMMARY

Developing strategies against the SARS-CoV-2 is currently a main research subject. SARS-CoV-2 infects host cells by binding to human ACE2 receptors. Both, virus and ACE2, are highly glycosylated, and exploiting glycans of the SARS-CoV-2 envelope as binding sites for ACE2 represents a virus strategy for attacking the human host. We report here that a family of mannose-binding synthetic carbohydrate-binding agents (CBAs) inhibits SARS-CoV-2 infection, showing broad neutralizing activity *vs.* several variants of the spike protein. Preliminary tests indicated that the investigated CBAs interact with the spike protein rather than with ACE2. For a lead compound (IDS060), which has been selected among others for its lack of cytotoxicity, evidence of binding to the RBD of the spike protein has been found by NMR experiments, while competitive binding assays in the presence of IDS060 showed inhibition of binding of RBD to hACE2, although neutralizing activity was also observed with variants showing reduced or depleted binding.

INTRODUCTION

The outbreak of the COVID-19 pandemic, caused by the SARS-CoV-2 virus, represents a critical health problem worldwide and an urgent clinical emergency. In terms of cumulative number of confined cases, the SARS-CoV-2 infection has largely exceeded the numbers reported during SARS-CoV and MERS-CoV period (Wang et al., 2020). It is well established that, like other coronaviruses, SARS-CoV-2 enters human cells by binding to the angiotensin-converting enzyme 2 (ACE2) receptor, exploiting the trimeric trans-membrane glycoprotein spike (S) for attachment (Tortorici and Veesler, 2019). The trans-membrane glycoprotein S, which protrudes from the viral surface, features two functional subunits: S1, that mediates the virus-host cell binding, and S2, which triggers the virus fusion with the host cell membrane (Walls et al., 2020). The S1 sub-unit features the "receptor-binding domain" (RBD) and participates in stabilization and fusion of the S2 sub-unit. The S2 sub-unit harbors the fusion peptide (FP) and plays an essential role in mediating membrane fusion of virus and host cell. Once adhesion to the cell is established, the S glycoprotein is cleaved by host cell proteases at the S2' site, the viral proteins are activated, and fusion occurs (Millet and Whittaker, 2015).

The S protein is highly glycosylated; protein glycans are important for the correct folding of the protein, and for modulating docking and fusion of the virus to the host cell (Walls et al., 2019), as well as for the steric hindrance induced on the spike (Huang et al., 2021). Indeed, glycans conceal aminoacidic residues and other epitopes, allowing the coronavirus to escape the immune system. Knowledge of the glycans involved in fusion at molecular level is, therefore, of paramount importance to elaborate strategies to prevent the cross-talking between virus and the host cell. Yet, research worldwide is currently fully focused on the inhibition of the interaction between the viral proteins S and the human hACE2 largely neglecting recognition at molecular level of specific glycan residues of the spike protein S by the hACE2 receptor, although the role of highly mannosilated glycans is becoming increasingly appreciated (Stravalaci et al., 2022; Sztain et al., 2021).

Currently, for 17 out of 22 sites of N-glycosylation of S1 and S2, the oligosaccharidic structure has been mapped (Shajahan et al., 2020), and a direct involvement of specific glycan terminal residues in the

[1]Dipartimento di Chimica, DICUS, University of Florence, Florence, Italy

[2]Fondazione INGM - Istituto Nazionale Genetica Molecolare "Romeo ed Enrica Invernizzi", Milan, Italy

[3]CERM, University of Florence, Florence, Italy

[4]Dipartimento di Scienze Farmacologiche e Biomolecolari, University of Milan, Milan, Italy

[5]INSTM, University of Florence, Florence, Italy

[6]These authors contributed equally

[7]Lead contact

*Correspondence: grifantini@ingm.org (R.G.), defrancesco@ingm.org (R.D.F.), cristina.nativi@unifi.it (C.N.)

https://doi.org/10.1016/j.isci.2022.104239

cell-to-virus adhesion has been reported (Tian et al., 2021; Pinto and Park, 2020; Watanabe et al., 2020). In particular, the highly mannosylated eptasaccharide $Man_5GlcNAc_2$, the nonasaccharide $Man_7GlcNAc_2$, and the decasaccharide $Man_8GlcNAc_2$ (Zhao P. et al., 2020) as well as oligosaccharides terminated with fucose residues (Shajahan et al., 2020), are among the glycans proposed as determinants in virus binding to ACE2. By using glycomic/glycoproteomic and molecular dynamic approaches (Zhao P. et al., 2020), the structure and role of glycans in the interaction between spike and ACE2 receptor was investigated, determining the occupancy and site-specific heterogeneity of N-linked glycans and O-linked glycosylation on spike and ACE2 receptor. The study also proposes different roles for glycans in receptor-viral binding and glycan shielding of spike. A deeper understanding of how these binding processes are involved in viral infection could lead to desperately needed antiviral agents, counteracting SARS-CoV-2 as well as other viral outbreaks (Bravo et al., 2021).

SARS-CoV-2, and coronaviruses in general, belongs to the membrane enveloped virus class, such as, among others, HIV-1 (Thompson et al., 2019). Like SARS-CoV-2, the HIV-1 virus is characterized by mannosides on the terminal oligosaccharides of the glycan shield. The oligomannosides on the HIV envelope facilitate the viral entry by binding to the receptor domain of the host cell protein DC-SIGN. In an original therapeutic concept for suppressing enveloped viruses (Balzarini, 2007), these glycans constitute the target of carbohydrate-binding agents (CBAs), as demonstrated, for example, for the antibiotic pradimicin A, showing antiviral activity against HIV-1. In line with this concept, targeting of N-linked glycans of the S glycoprotein envelope of SARS-CoV-2 via CBAs has recently been proposed as an attractive therapeutic approach for developing antivirals (Gupta et al., 2020).

In the last decade, we have developed a family of synthetic aminopyrrolic receptors, *i.e.*, small abiotic molecules that proved to be effective as CBAs, showing antibiotic activity against pathogenic yeasts (Nativi et al., 2012). A general correlation was found between their activity and their binding ability toward mannosides, which are densely expressed on the cell wall of these pathogens. Tested for antiviral activity, these molecules have been shown to effectively inhibit the HIV infection. Comparison of their binding properties toward the HIV glycoproteins, as revealed by surface plasmon resonance (SPR) experiments, and their binding affinities for mannosides revealed a direct correlation, supporting the notion that antiviral activity may be triggered by the recognition of the highly mannosylated glycoprotein gp120 of the viral envelope, featuring the $Man_9GlcNAc_2$ epitope, which is crucial for the HIV infection (Francesconi et al., 2015; Ciaco et al., 2020). Furthermore, this family of CBAs was found to induce apoptotic cell death, which reflected their ability to bind mannose glycans displayed on the cell surface, in a way much alike that observed in cells treated with mannose-binding concanavaline-A (ConA) (Park et al., 2015).

Based on the above previous studies, because the $Man_9GlcNAc_2$ glycan of the HIV gp120 is structurally related to the $Man_5GlcNAc_2$ epitope of the SARS-CoV-2 virus, the present work has been specifically focused to ascertain whether the set of aminopyrrolic structures developed as CBAs may possibly exhibit inhibition properties vs. the SARS-CoV-2 entry, most likely by recognition of the high-mannose type glycans expressed on the spike protein, which mediate the virus-host cell binding and are involved in the infection process. The basic idea is that the mannoside epitopes of the spike protein, when bound to the synthetic receptor, may not be available for binding to hACE2, thus preventing adhesion and infection.

RESULTS AND DISCUSSION

The set of synthetic receptors selected to target the highly mannosylated glycans expressed on the spike protein was chosen among those compounds that showed the strongest interaction with the highly mannosylated glycoprotein gp120 of HIV (Francesconi et al., 2015). The synthetic receptors depicted in Figure 1 belong to the aminopyrrolic family of carbohydrate-binding agents (CBA), which recognize mannosides through a combination of CH-π and hydrogen-bonding interactions. The set consists of two pairs of enantiomeric compounds (OFR626/OFR622 and OFR971/GGA328), and of an achiral molecule (IDS060), all of which are slightly soluble in water at neutral pH, due to partial protonation of the secondary amines.

Effect of carbohydrate-binding agents on SARS-CoV-2 pseudovirus infection

To test the potential antiviral activity of the selected CBAs on SARS-CoV-2 infection, we developed a pseudovirus assay based on lentiviral particles pseudotyped with spike protein. Pseudovirus systems have been successfully used to recapitulate cell entry both for SARS-CoV and SARS-CoV-2 (Hofmann et al., 2004; Simmons et al., 2004; Ou et al., 2020). They represent a safe and rapid tool to investigate cell factors involved in

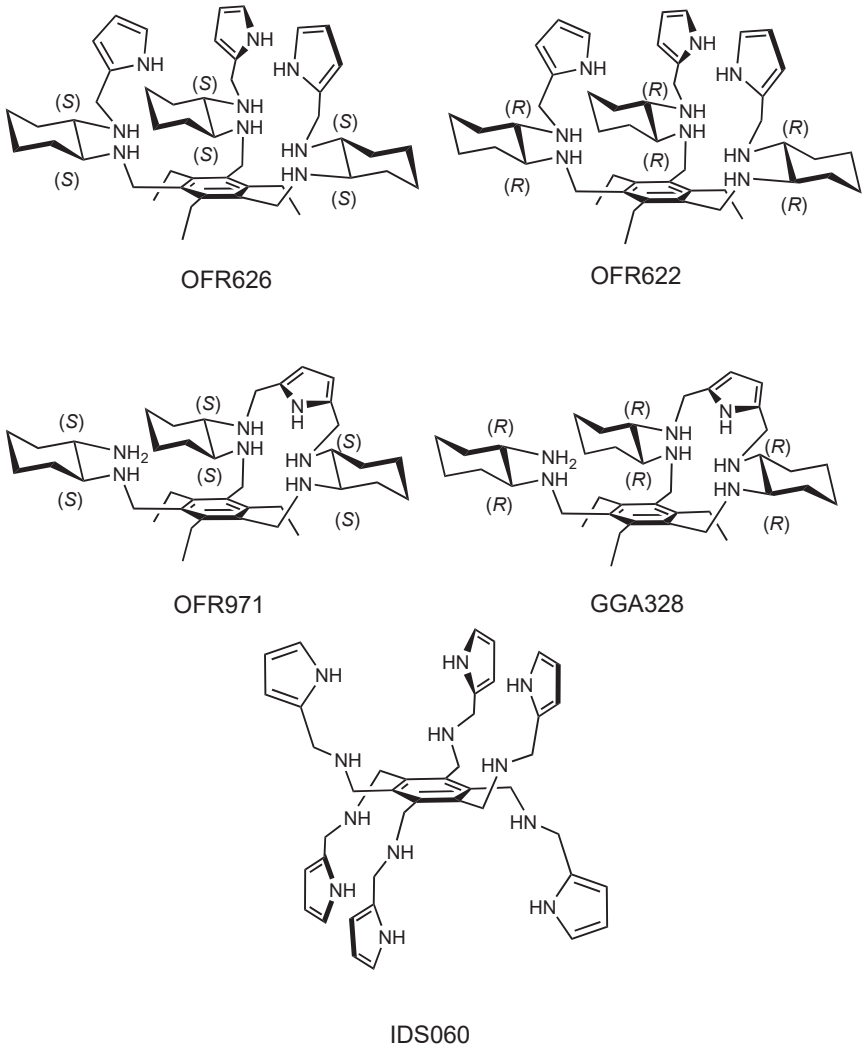

Figure 1. Structure of the investigated carbohydrate-binding agents

cell entry and to identify small molecules or antibodies that block infection, either targeting viral spike or hACE2. To generate lentiviral pseudotyped particles, the VSV-G protein of vesicular stomatitis virus was replaced by the SARS-CoV-2 spike protein. To quantitively measure cell entry, the lentiviral pseudoparticles were engineered with luciferase reporter gene.

The CBAs reported in Figure 1 were first tested at a single concentration of 10 μM. As recipient cells, we used a HEK293T cell line engineered for the expression of hACE2 (HEK293T-hACE2). Pseudoparticles were preincubated with CBAs at 37°C for 1 h and then used to infect HEK293T-hACE2 at 0.1, 0.3, 0.5, and 1.0 multiplicity of infection (MOI). After 24 h incubation, cell infection was measured by the luciferase assay, whereas cytotoxicity was evaluated by a cell viability assay. An anti-spike RBD antibody was used as a positive control of infection inhibition. Figure 2 shows the inhibition and cytotoxicity effects of each tested molecule. Compound IDS060 showed clear effects on pseudovirus infection (Figure 2A), reducing the infection by 50% under all tested conditions, together with lack of significant cytotoxicity (Figure 2B). OFR622, OFR626, and OFR971, conversely, completely neutralized pseudovirus infection (Figure 2A), but their efficacy was associated with a marked cytotoxic effect (Figure 2B). GGA328 showed a somewhat intermediate behavior, reducing the infection by 80%, but showing a significant cytotoxic effect. The latter four molecules were tested at lower concentration (1 μM), to assess whether inhibition of infection could be observed in the absence of cytotoxicity (Figures 2C and 2D). Results indicate that the inhibitory effect of these molecules paralleled cytotoxicity, pointing to a nonspecific mechanism of inhibition.

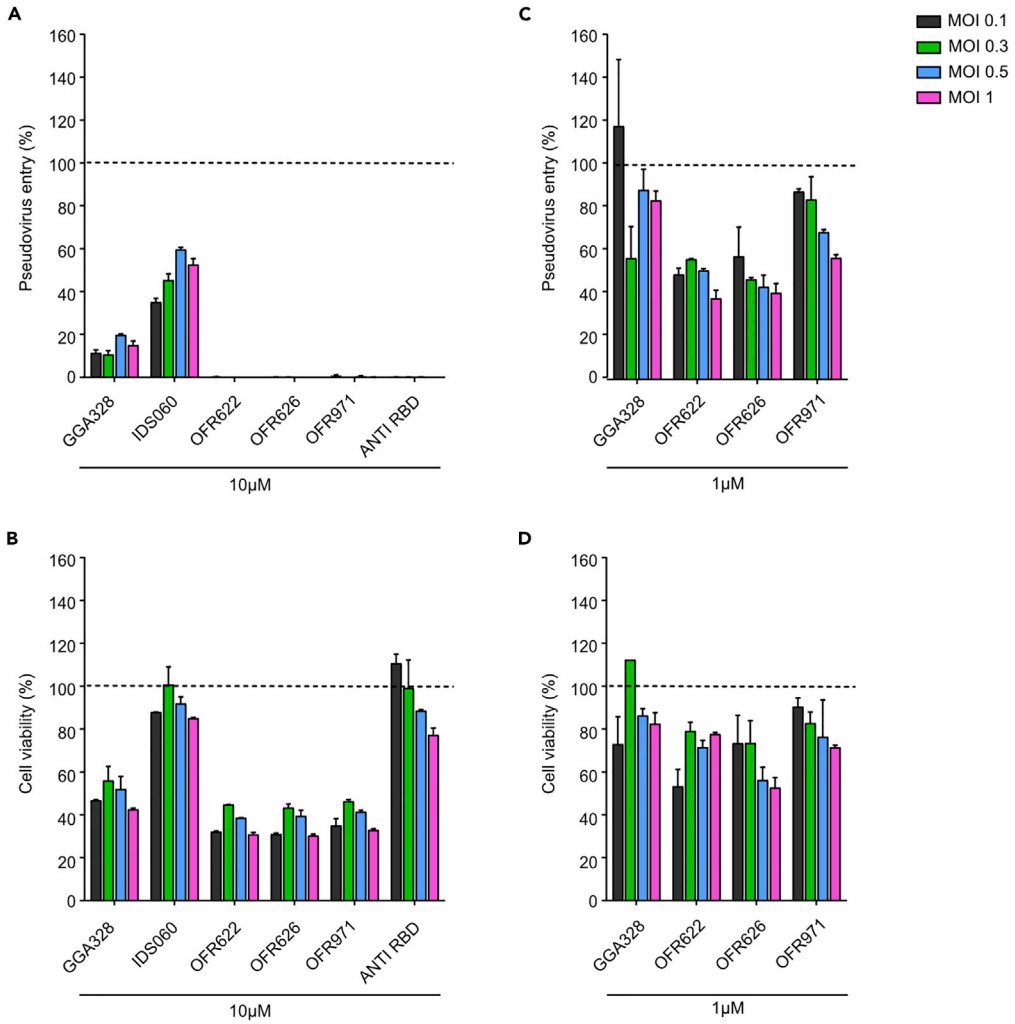

Figure 2. Effect of carbohydrate-binding agents on SARS-CoV-2 pseudovirus infection by interaction with the spike protein

Histograms representing neutralization activity against SARS-CoV-2 pseudovirus infection (A, C) and cytotoxic effect (B, D) of different CBAs at 10 μM (A, B) and 1 μM (C, D). Data are plotted as mean values ± standard deviation of three experimental replicates and normalized to untreated samples (indicated as 100%). An anti-spike RBD antibody was used at 1:100 dilution as a control of infection inhibition. MOI: multiplicity of infection.

Because the hACE2 receptor is also highly glycosylated (Shajahan et al., 2021), we considered the possibility that CBAs may act as inhibitors of infection by binding to the receptor rather than to the virus. To test this possibility, we designed a screening experiment in which cells were pre-incubated with the CBAs and challenged afterwards with the pseudovirus. In this type of experiment, the very high level of hACE2 expression present in HEK293T-hACE2 engineered cells could lead to a decreased inhibition effect of the ligand. Thus, we set out to evaluate the ability of the CBAs to inhibit pseudovirus infection in the hepatoma-derived Huh7.5 cell line. HuH7.5 cells line constitutively express the hACE2 receptor at levels that are significantly lower than those observed in HEK293T-hACE2 (data not shown) and can be efficiently infected by the spike lentiviral pseudotyped particles. Because of the lower hACE2 levels expressed by HuH7.5, compared to the previous experiment, higher MOI was used for infection, and the reporter gene activity was measured at a longer time. CBAs (10 μM) were preincubated with HuH7.5 cells for 1 h at 37°C and then cells were infected at MOI of 1 or 10. An anti-hACE2 antibody (20 μg/mL) was used as control for neutralization of infection. Cell infection luciferase activity and cytotoxicity were measured after further 48 h incubation. Figure 3 shows that none of the tested CBAs showed inhibition of infection in absence of cytotoxicity (Figures 3A

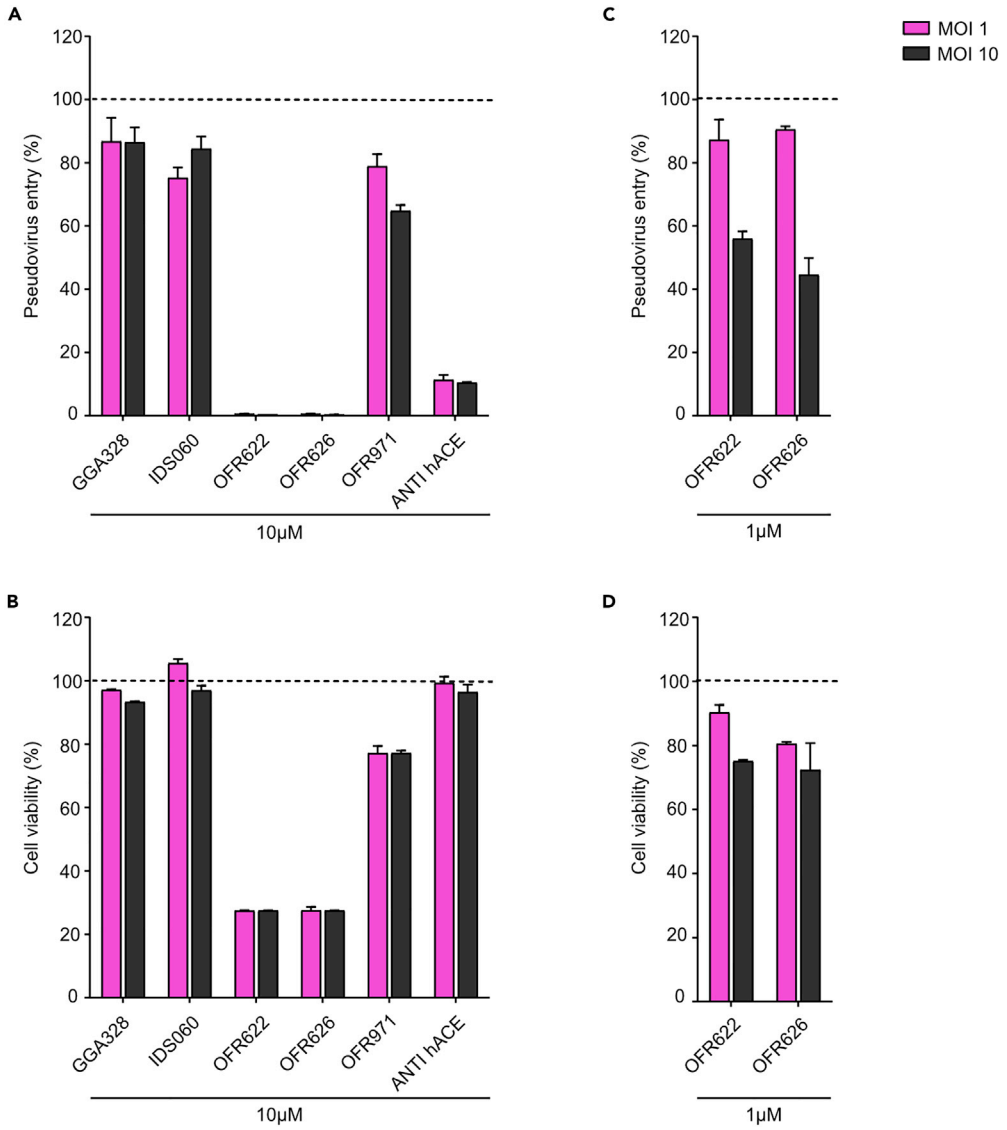

Figure 3. Effect of carbohydrate-binding agents on SARS-CoV-2 pseudovirus infection by interaction with the hACE2 receptor

Histograms representing neutralization activity against SARS-CoV-2 pseudovirus infection (A, C) and cytotoxic effect (B, D) of different CBAs at 10 μM (A, B) and 1 μM (C, D). Data are plotted as mean values ± standard deviation of three experimental replicates and normalized to untreated samples (indicated as 100%). MOI: multiplicity of infection.

and 3B). OFR622 and OFR626, which were cytotoxic at 10μM, were also tested at 1μM, but did not show useful inhibitory activity in either infection condition (Figures 3C and 3D).

The lack of inhibitory activity of IDS060 when bound to the hACE2 receptor supports the notion that interaction with the viral spike protein is most likely responsible for its inhibitory activity. Therefore, only IDS060 was selected for further characterization.

IDS060 is a dose-dependent inhibitor of SARS-CoV-2 pseudovirus infection and its activity is maintained across spike variants of concern

Dose-response experiments were performed with IDS060 to confirm the effects observed by the single-dose inhibition experiments. HEK293T-hACE2 were infected with different MOI of pseudoparticles that were previously preincubated with increasing concentration of IDS060 (1 h at 37°C). IDS060 showed a

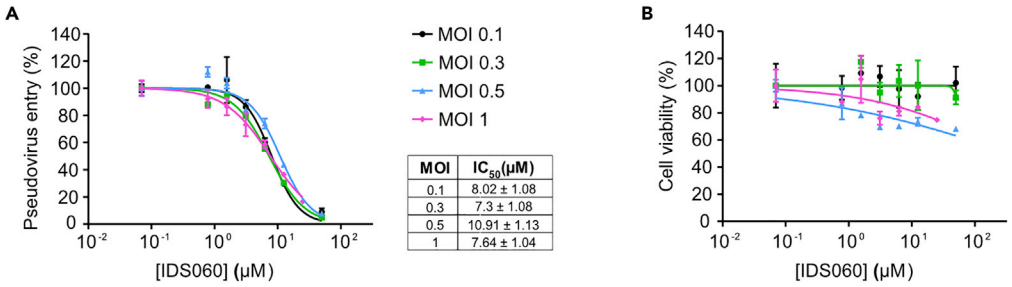

Figure 4. Neutralizing activity of IDS060 against SARS-CoV-2 pseudovirus infection

(A) Dose-response curves representing the IDS060 neutralization activity against SARS-CoV-2 pseudovirus infection at different MOI, and (B) corresponding cytotoxic effect. Data are plotted as mean values ± standard deviation of three experimental replicates and normalized on untreated samples (indicated as 100%). Non-linear regression fitting curves are represented as color solid lines. The IC_{50} values (μM) are reported in the table for different pseudovirus MOI (multiplicity of infection).

dose-dependent inhibition of infection at MOIs not associated with any cytotoxicity (Figure 4 a and b) with IC_{50} values of 8.02 μM (MOI 0.15) and 7.3 μM (MOI 0.3). Experiments at higher MOI revealed similar IC_{50} values, albeit with moderate cytotoxicity at the higher compound concentrations (Figrue 4b).

In March 2020, a spike variant characterized by a single amino acid mutation—aspartate to glycine substitution at position 614 (D614G)—appeared and gradually outcompeted the original pandemic SARS-CoV-2 strain, becoming the prevalent circulating variant (Hu et al., 2020). This variant is more transmissible, thus providing the virus with a selective advantage over the original strain. Other single point spike mutations, reported to arise in several additional circulating variants, are considered of particular concern, because they could increase viral infectivity or evade SARS-CoV-2 neutralizing antibodies. In particular, the spike N501Y mutation seems to increase infection efficiency by more tightly binding to the hACE2 receptor, and the E484K and N439K mutations are considered escape mutants that can helps virus in evading antibodies.

IDS060 was tested for its ability to neutralize infection of a panel of pseudoviruses carrying selected single-residue mutation (Figure 5). Results indicate that IDS060 shows inhibitory activity across all the mutants with comparable IC_{50} values. Therefore, neither the more infectious D614G and N501Y nor the antibody escape mutants E484K and N439K, impact on the antiviral effect of IDS060, showing the high clinical potential of this CBA.

Over the course of the pandemic, different variants of SARS-CoV-2 have arisen. Currently, five main variants of SARS-CoV-2—namely, B.1.1.7 (α), B.1.351 (β), P.1 (γ), B.1.617.2 (δ), and B.1.529 (ο)—are raising concern. The newly emerged SARS-CoV-2 lineage called B.1.1.7 (α), or UK variant, was detected in Kent, England, in December 2020 and was reported to spread more efficiently and faster than other strains. This mutant contains 7 amino acid mutations and 2 deletions in the spike protein; among these, the N501Y mutation was shown to give increased ACE2 binding affinity (Zhu et al., 2021). The South African lineage B.1.351 (β) and the Brazil variants P.1 (γ) contain 10 and 11 single point mutations in the spike sequence, respectively; specifically, the RBD N501Y, E484K, and K417T mutations are common to the two variants. Importantly, the set of mutations shared by P.1 and B.1.1.7 lineages appear to have emerged entirely independently, raising concern about convergent evolution to a new phenotype, potentially associated with an increase in transmissibility and/or escape to natural immunity. The variant B.1.617.2 (δ) was discovered in India in late 2020 and spread worldwide becoming nowadays the most dominant strain. It contains 9 mutations in the spike protein sequence (according to https://outbreak.info), among which T478K and L452R, involved in binding affinity for hACE2 receptor and immune evasion, and P681R, located in the furin cleavage site, that facilitates furin-mediated cleavage of the S protein. Globally, the Delta (δ) variant appears to have more transmissibility as well as a slightly reduced susceptibility to neutralizing antibodies from either convalescent or vaccinated plasma. Moreover, this variant has been associated to increases risk of hospitalization. The Omicron (ο) variant was detected in South Africa in early November 2021. It contains 30 mutations in the spike protein, 15 of which located in RBD. These changes in amino acid composition lock the RBD in the "down" conformation and lead to a marked reduction of immune protection in convalescent and vaccinated individuals, and to a complete resistance to neutralization by monoclonal antibodies directed to the RBD.

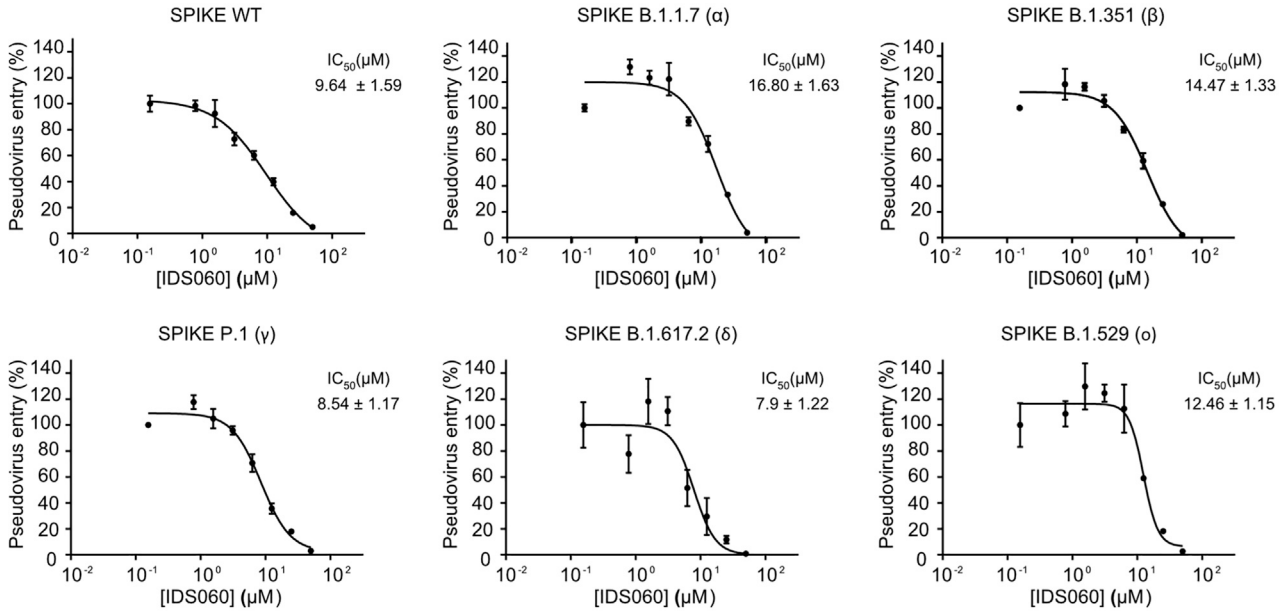

Figure 5. Neutralizing activity of IDS060 against SARS-CoV-2 pseudovirus featuring single point mutations

Dose-response curve representing IDS060 neutralization activity against different single point mutants of spike. Data are plotted as mean values ± standard deviation of three experimental replicates and normalized on untreated samples (indicated as 100%). Non-linear regression fitting curves were represented as solid lines. The IC_{50} values (μM) for each spike mutant are indicated in each plot. WT: wild type spike sequence QHD43416.1.

IDS060 was tested for neutralizing activity against pseudoviruses harboring the spike from the main variants of concern. Our results (Figure 6) indicate that activity is maintained, and neutralization potency is conserved between the wild-type spike and the variants of concerns, with IC_{50} values ranging between 8 and 17 μM, suggesting a generally broad activity of IDS060 against SARS-CoV-2 variants.

IDS060 acts as inhibitor of SARS-CoV-2 infection

To validate the antiviral effect of IDS060 on SARS-Cov-2, the neutralization activity was assayed in an *in vitro* infection system with wild-type SARS-CoV-2 virus. SARS-CoV-2 infection was performed using the human lung cancer cell line Calu-3 that has been widely reported to be susceptible to SARS-CoV-2 infection and represents the physiological cellular tropism of SARS-CoV-2 during human infection (Chu et al., 2020). Like with pseudovirus, SARS-CoV-2 viral inoculum was preincubated with 50 μM IDS060 at 37°C for 30 min, and then used to infect Calu-3 at 0.1 and 1 MOI. After 24 h of incubation, cell infection was measured by SARS-CoV-2-specific real-time PCR, while cytotoxicity was evaluated by a cell viability assay. The anti-spike RBD antibody was used as positive control for the experiment. Figure 7 shows that IDS060 reduced the infection of approximately 80% and 60% at 0.1 and 1 MOI, respectively (Figure 7A), devoid of any cytotoxic effect (Figure 7B). The potency of inhibition observed at 0.1 and 1 MOI can be directly correlated to the different number of viral particles. The higher inhibition efficacy observed, compared to the pseudovirus infection, can be related to several factors affecting the results obtained by surrogate viruses, such as the density of spike expressed on the pseudovirus envelope, or their replication defectiveness. Apart from the difference between the two systems, the result obtained using the wild-type virus confirms and validates the antiviral effect of IDS060, thus highlighting a new class of molecules that can be further investigated in the drug development research for COVID-19.

NMR binding experiments of IDS060 vs receptor-binding domain (RBD)

Because the SARS-CoV2 infection is ascribed to the interaction of the RBD of the spike protein with the ACE2 receptor, we investigated whether the inhibitory effect exhibited by IDS060 could be ascribed to binding of the latter to RBD. To this end, unambiguous evidence of binding of IDS060 on recombinant RBD wt could be obtained by NMR spectroscopy. The folding state of the protein was assessed by analysing the distribution of amide and methyl proton resonances outside the random coil chemical shift regions in a 1D ^{1}H NMR spectrum (Figure S3), which showed that the spreading of signals is consistent with

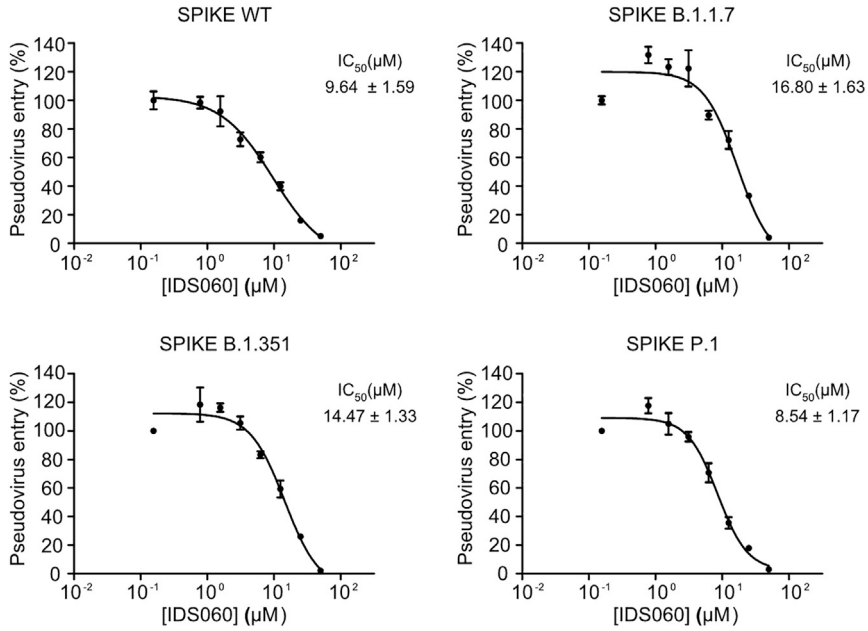

Figure 6. Neutralizing activity of IDS060 against SARS-CoV-2 pseudovirus featuring circulating variants of spike

Dose-response curves representing IDS060 neutralization activity against different circulating variants of spike. Data are plotted as mean values ± standard deviation of three experimental replicates and normalized on untreated samples (indicated as 100%). Non-linear regression fitting curves were represented as solid lines. IC_{50} values (μM) are indicated for each spike mutant pseudovirus. WT: wild-type spike sequence QHD43416.1.

a well-structured protein. The large molecular weight of the RBD and the use of mammalian cells as expression system make the use of protein-based NMR screening extremely challenging. Therefore, binding of IDS060 to RBD was investigated through a ligand-based approach by saturation transfer difference (STD) NMR experiments (Mayer and Mayer, 1999), in which the interaction is monitored through non-scalar magnetization transfer from the protein to the small synthetic molecule. In STD experiments, saturation of the protein signals, in a region far away from ligand signals, is efficiently transferred by spin diffusion to the bound ligand; saturation of the bound ligand is then spread by chemical exchange over the large excess of free ligand in solution, where is monitored because of the very different relaxation times with respect to the protein. As a result, due to the transmitted saturation, the signals of the ligand interacting with the protein experience a decrease in intensity, which is easily detected in a difference spectrum, whereas any unbound species will be canceled out from the spectrum. STD experiments are extremely sensitive and reliable, allowing the identification of bound ligands with K_D in the range of 10^{-3}–10^{-8} (Meyer and Peters, 2003). In our study, the experiment was performed on an 800 μM solution of IDS060, in the presence of RBD at 20 μM concentration. In Figure 8, it can be easily appreciated that the signals of the pyrrole moieties and of the CH_2 connecting arms of the ligand are observed, in the difference spectrum, in the presence but not in the absence of RBD, unambiguously demonstrating that IDS060 is bound to the RBD of the spike protein.

IDS060 directly interferes with RBD binding to hACE2 in HuH7.5 cells

Relying on NMR results, we investigated whether the IDS060 inhibitory activity toward the SARS-CoV-2 pseudovirus and virus infection may be ascribed to inhibition of binding of RBD to hACE2 receptors. We carried out a competitive binding assay by incubating the protein with HuH7.5 cells with recombinant conjugated-AF/647 RBD (Figure S2 and STAR Methods) in the presence of increasing concentration of IDS060 (0–10μM) and measuring the surface binding of RBD to hACE2 by flow cytometry analysis. We found that IDS060 significantly reduced binding, showing an IC_{50} value of 5 μM (Figure 9). We further investigated whether the IDS060 binding inhibition is maintained across RBDs derived from the variants of current interest, i.e., B.1.1.7, B.1.351, and P1. Compared to RBD wild type, IDS060 displayed a lower binding inhibition vs. RBD-B.1.1.7, whereas did not inhibit binding of RBD-B.1.351 and of RBD-P1 (see Figure S3 and STAR Methods). Intriguingly, the reduced (vs. RBD-B.1.1.7) or depleted (vs. RBD-B.1.351 and RBD-P1) binding inhibition activity observed for IDS060 is consistent with recently published neutralization data reported for

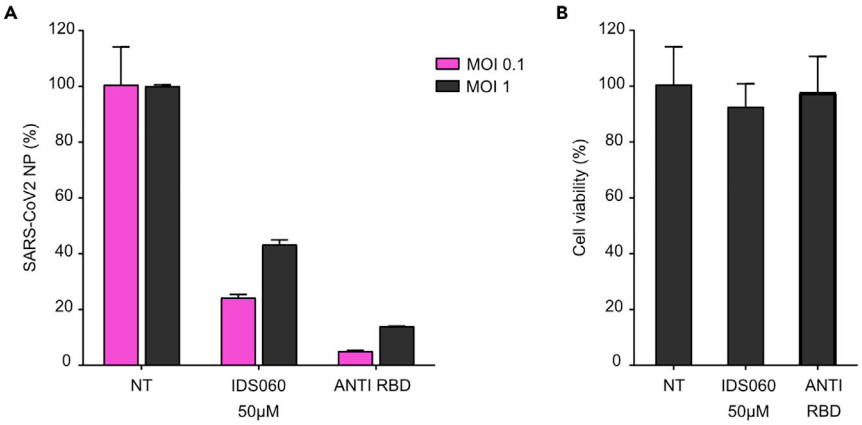

Figure 7. Antiviral activity of IDS060 against SARS-CoV-2 wild-type virus

(A) Histograms representing antiviral activity against SARS-CoV-2 wild-type virus and (B) cytotoxic effect of IDS060 at 50 μM. Data are plotted as mean values ± standard deviation of two experimental replicates and normalized to NT (infected untreated sample). An anti-spike RBD antibody was used at 1:100 dilution as a control of infection inhibition. MOI: multiplicity of infection.

N-terminal domain- and RBD-directed antibodies vs. the same variants (Gobeil et al., 2021; Zhao et al., 2020a, 2020b), which were associated with increased binding to ACE2, mediated by higher propensity for RBD-up states, related to allosteric effects affecting the spike conformation. Because infection by SARS-CoV-2 is effectively inhibited by IDS060 even for variants showing decreased or depleted binding inhibition of RBD to the hACE2 receptor, our results suggest that the antiviral activity of IDS060 may be due not only to the inhibition of binding of RBD to hACE2 but also to the interaction with glycans, likely mannosides, exposed outside the receptor-binding domain, but located in regions of the spike protein where they may induce conformational changes. Overall, the broadly inhibitory activity of IDS060 may be consistent with recently reported information suggesting that the spike protein may achieve different conformations in SARS-CoV-2 variants, with the consequent alteration of RBD up/down state (Cai et al., 2020; Casalino et al., 2020).

CONCLUSIONS

A new class of carbohydrate-binding agents (CBAs) capable of inhibiting SARS-CoV-2 infection by hampering the entry step of the viral cell life has been described. One member of the investigated set of CBAs, namely IDS060, showed significant inhibition activity devoid of toxicity, whereas other members, although very effective, showed toxicities too high to be usefully exploited. While activity appears to be mainly due to binding of IDS060 to RBD of the wild-type spike protein, which in turn inhibits binding of the latter to the ACE2 receptor, antiviral activity is still observed with variants for which binding to RBD is poor or absent. This evidence suggests that IDS060 may also bind to sites of the spike other than the RBD, where it may induce conformational changes that inhibit infection. SARS-CoV-2 infection is known to be controlled by the opening of the glycan-shielded RBD to an "up" state, which is the active form binding to the human ACE2 receptor. Because the spike protein is heavily glycosylated, with high-mannose type glycans largely represented, and because the investigated CBA family has been shown to recognize mannosides, it is suggested that binding to the spike protein may be due to recognition of the mannosylated glycans on its surface. In this context, it has recently been shown (Sztain et al., 2021) that the N-glycan at position N343, which consists of glycans ranging from $Man_5GlcNAc_2$ to $Man_9GlcNAc_2$, plays a gating role in RBD opening to the "up" state: an appealing hypothesis, therefore, is that binding of IDS060 to the N343 glycan may prevent opening of the RBD and binding to the ACE2 receptor. The preliminary results reported herein can be leveraged to develop new CBAs, based on the IDS060 structure, that may exhibit higher neutralization potency and lead to future candidate drugs for treating the SARS-CoV-2 infection. Structural modifications are currently under way to this purpose.

Limitations of the study

In addition to NMR STD evidence, experimental evidence to support the hypothesis of IDS060 binding to the spike protein is currently sought by cryo-EM studies. At present, binding of IDS060 to high-mannose-type

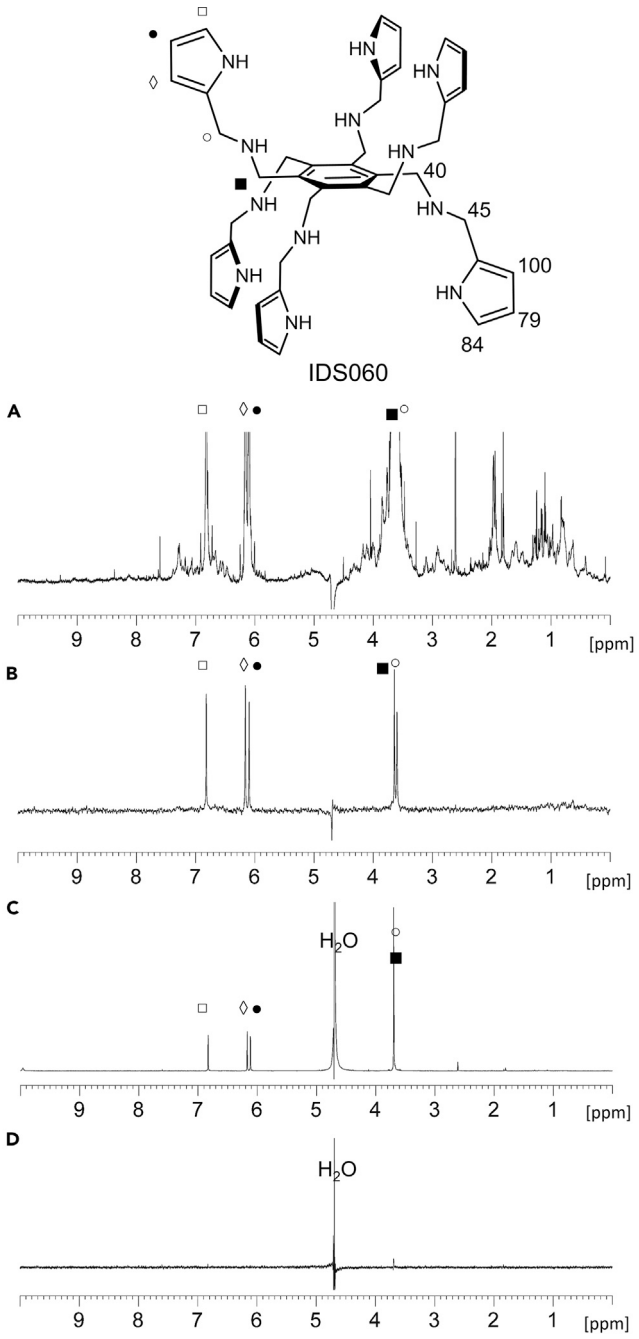

Figure 8. Binding of IDS060 to the RBD of the spike protein by saturation transfer difference (STD) experiments

^{1}H NMR spectra of IDS060 (800 μM) in the presence (A And B) and in the absence (C And D) of RBD (20 μM). (A) Reference spectrum of IDS060 + RBD saturated off-resonance at $\delta = -40$ ppm. The spectrum, showing signals from both partners, was scaled up to the protein intensity; (B) Difference spectrum (STD) between IDS060 + RBD saturated off-resonance at $\delta = -40$ ppm, and on-resonance at $\delta = -2$ ppm; (C) Reference spectrum of IDS060 saturated off-resonance at $\delta = -40$ ppm; (D) difference spectrum (STD) between IDS060 saturated off-resonance at $\delta = -40$ ppm, and on-resonance at $\delta = -2$ ppm. Signals assignment of IDS060 are indicated in the spectra, together with relative saturation (%) observed for the amino pyrrolic protons, normalized to the most intense STD signal. Residual signals of IDS060 are evident in the difference spectrum in the presence of RBD, due to saturation transfer from the protein, but are depleted in the absence of the protein, demonstrating unambiguous evidence of binding.

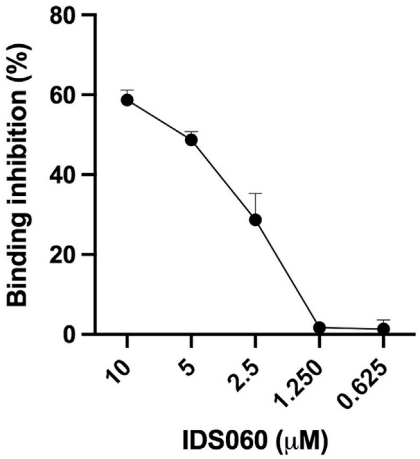

Figure 9. Competitive binding of IDS060 against RBD on HUH7.5 cells

Graph representing flow cytometry analysis of the ability of IDS060 to inhibit binding of recombinant RBD on HuH7.5 cells. The cells were treated with increasing concentrations of IDS060 (0–10 μM) and incubated with recombinant conjugated-AF/647 RBD. Data represent mean values ± standard deviation of three experimental replicates and normalized to cells incubated with RBD AF/647 in the absence of IDS060 (considered as 100% of binding).

glycans of the spike protein is only proposed on the basis of previous findings correlating affinities of amino-pyrrolic CBAs for mannosides with antiviral, antimicotic, and apoptotic activities, but supporting evidence needs to be found in the present case. Although the described preliminary results appear promising in terms of antiviral activity and lack of cytotoxicity, further investigation is required to ascertain the actual mechanism of action and assess the full toxicity profile of this class of CBAs, as a requirement for further preclinical development.

STAR★METHODS

Detailed methods are provided in the online version of this paper and include the following:

- KEY RESOURCES TABLE
- RESOURCE AVAILABILITY
  - Lead contact
  - Materials availability
  - Data and code availability
- EXPERIMENTAL MODEL AND SUBJECT DETAILS
  - Cells
  - Plasmids
  - Viral strain
- METHODS DETAILS
  - HEK293TN-hACE2 generation
  - SARS-CoV-2 pseudotype particles generation
  - Neutralization assays
  - Cloning, expression, and purification of recombinant SARS-CoV-2 proteins
  - Competitive binding assay
  - NMR spectroscopy
  - Propagation of SARS-CoV-2 and *in vitro* infection
- QUANTIFICATION AND STATISTICAL ANALYSIS

SUPPLEMENTAL INFORMATION

Supplemental information can be found online at https://doi.org/10.1016/j.isci.2022.104239.

ACKNOWLEDGMENTS

Funding: Ministero dell'Università e della Ricerca (Miur) of Italy (project n. FISR2020IP_01095).

AUTHOR CONTRIBUTIONS

Conceptualization: OF, LD, MF, SR; Investigation: OF, LD, MF, EP, MB, AF, LM, MC; Supervision: RG, RDF, CN; Writing—original draft: RG, RDF, and CN; Writing—review & editing: SR

DECLARATION OF INTERESTS

The authors declare no competing interests

Received: November 10, 2021
Revised: March 21, 2022
Accepted: April 6, 2022
Published: May 20, 2022

REFERENCES

Balzarini, J. (2007). Targeting the glycans of glycoproteins: a novel paradigm for antiviral therapy. Nat. Rev. Microbiol. *5*, 583–597. https://doi.org/10.1038/nrmicro1707.

Bravo, M.F., Lema, M.A., Marianski, M., and Braunschweig, A.B. (2021). Flexible synthetic carbohydrate receptors as inhibitors of viral attachment. Biochemistry *60*, 999–1018. https://doi.org/10.1021/acs.biochem.0c00732.

Cai, Y., Zhang, J., Xiao, T., Peng, H., Sterling, S.M., Walsh, R.M., Jr., Rawson, S., Rits-Volloch, S., and Chen, B. (2020). Distinct conformational states of SARS-CoV-2 spike protein. Science *369*, 1586–1592. https://doi.org/10.1126/science.abd4251.

Casalino, L., Gaieb, Z., Goldsmith, J.A., Hjorth, C.K., Dommer, A.C., Harbison, A.M., Fogarty, C.A., Barros, E.P., Taylor, B.C., McLellan, J.S., et al. (2020). Beyond shielding: the roles of glycans in the SARS-CoV-2 spike protein. ACS Cent. Sci. *6*, 1722–1734. https://doi.org/10.1021/acscentsci.0c01056.

Chu, H., Chan, J.F.-W., Yuen, T.T.-T., Shuai, H., Yuan, S., Wang, Y., Hu, B., Yip, C.C.-Y., Tsang, J.O.-L., Huang, X., et al. (2020). Comparative tropism, replication kinetics, and cell damage profiling of SARS-CoV-2 and SARS-CoV with implications for clinical manifestations, transmissibility, and laboratory studies of COVID-19: an observational study. Lancet Microbe. *1*, e14–e23. https://doi.org/10.1016/S2666-5247(20)30004-5.

Ciaco, S., Humbert, N., Real, E., Boudier, C., Francesconi, O., Roelens, S., Nativi, C., Seguin-Devaux, C., Mori, M., and Mély, Y. (2020). A class of potent inhibitors of the HIV-1 nucleocapsid protein based on aminopyrrolic scaffolds. ACS Med. Chem. Lett. *11*, 698–705. https://doi.org/10.1021/acsmedchemlett.9b00558.

Francesconi, O., Nativi, C., Gabrielli, G., De Simone, I., Noppen, S., Balzarini, J., Liekens, S., and Roelens, S. (2015). Antiviral activity of synthetic aminopyrrolic carbohydrate-binding agents: targeting the glycans of viral gp120 to inhibit HIV entry. Chem. Eur. J. *21*, 10089–10093. https://doi.org/10.1002/chem.201501030.

Gobeil, S.M.-C., Janowska, K., McDowell, S., Mansouri, K., Parks, R., Stalls, V., Kopp, M.F., Manne, K., Li, D., Wiehe, K., et al. (2021). Effect of natural mutations of SARS-CoV-2 on spike structure, conformation, and antigenicity. Science *373*, 641. https://doi.org/10.1126/science.abi6226.

Gupta, R.K., Apte, G.R., Lokhande, K.B., Mishra, S., and Pal, J.K. (2020). Carbohydrate-binding agents: potential of repurposing for COVID-19 therapy. Curr. Protein Pept. Sci. *21*, 1085–1096. https://doi.org/10.2174/1389203721666200918153717.

Hofmann, H., Geier, M., Marzi, A., Krumbiegel, M., Peipp, M., Fey, G.H., Gramberg, T., and Pöhlmann, S. (2004). Susceptibility to SARS coronavirus S protein-driven infection correlates with expression of angiotensin converting enzyme 2 and infection can be blocked by soluble receptor. Biochem. Biophys. Res. Commun. *319*, 1216–1221. https://doi.org/10.1016/j.bbrc.2004.05.114.

Hu, J., He, C.-L., Gao, Q.Z., Zhang, G.-J., Cao, X.-X., Long, Q.-X., Deng, H.-J., Huang, L.-Y., Chen, J., Wang, K., et al. (2020). D614G mutation of SARS-CoV-2 spike protein enhances viral infectivity. Preprint at BioRxiv. https://doi.org/10.1101/2020.06.20.161323.

Huang, C., Tan, Z., Zhao, K., Zou, W., Wang, H., Gao, H., Sun, S., Bu, D., Chai, W., and Li, Y. (2021). The effect of *N*-glycosylation of SARS-CoV-2 spike protein on the virus interaction with the host cell ACE2 receptor. iScience *24*, 103272. https://doi.org/10.1016/j.isci.2021.103272.

Mayer, M., and Meyer, B. (1999). Characterization of ligand binding by saturation transfer difference NMR spectroscopy. Angew. Chem. Int. Ed. *38*, 1784–1788. https://doi.org/10.1002/(SICI)1521-3773(19990614)38:12<1784::AID-ANIE1784>3.0.CO;2-Q.

Meyer, B., and Peters, T. (2003). NMR spectroscopy techniques for screening and identifying ligand binding to protein receptors. Angew. Chem. Int. Ed. *42*, 864–890. https://doi.org/10.1002/anie.200390233.

Millet, J.K., and Whittaker, G.R. (2015). Host cell proteases: critical determinants of coronavirus tropism and pathogenesis. Virus. Res. *202*, 120–134. https://doi.org/10.1016/j.virusres.2014.11.021.

Nativi, C., Francesconi, O., Gabrielli, G., De Simone, I., Turchetti, B., Mello, T., Di Cesare Mannelli, L., Ghelardini, C., Buzzini, P., and Roelens, S. (2012). Aminopyrrolic synthetic receptors for monosaccharides: a class of carbohydrate-binding agents endowed with antibiotic activity versus pathogenic yeasts. Chem. Eur. J. *18*, 5064–5072. https://doi.org/10.1002/chem.201103318.

Notarbartolo, S., Ranzani, V., Bandera, A., Gruarin, P., Bevilacqua, V., Putignano, A.R., Gobbini, A., Galeota, E., Manara, C., Bombaci, M., et al. (2021). Integrated longitudinal immunophenotypic, transcriptional and repertoire analyses delineate immune responses in COVID-19 patients. Sci. Immunol. *2021*, 6. https://doi.org/10.1126/sciimmunol.abg502110.1126.

Ou, X., Liu, Y., Lei, X., Li, P., Mi, D., Ren, L., Guo, L., Guo, R., Chen, T., Hu, J., et al. (2020). Characterization of spike glycoprotein of SARS-CoV-2 on virus entry and its immune cross-reactivity with SARS-CoV. Nat. Commun. *11*, 1620. https://doi.org/10.1038/s41467-020-15562-9.

Park, S.-H., Choi, Y.P., Park, J., Share, A., Francesconi, O., Nativi, C., Namkung, W., Sessler, J.L., Roelens, S., and Shin, I. (2015). Synthetic aminopyrrolic receptors have apoptosis inducing activity. Chem. Sci. *6*, 7284–7292. https://doi.org/10.1039/c5sc03200h.

Pinto, D., and Park, Y.-J. (2020). Cross-neutralization of SARS-CoV-2 by a human monoclonal SARS-CoV antibody. Nature *583*, 290–295. https://doi.org/10.1038/s41586-020-2349-y.

Shajahan, A., Archer-Hartmann, S., Supekar, N.T., Gleinich, A.S., Heiss, C., and Azadi, P. (2021). Comprehensive characterization of N- and O-glycosylation of SARS-CoV-2 human receptor angiotensin converting enzyme. Glycobiology *31*, 410–424. https://doi.org/10.1093/glycob/cwaa101.

Shajahan, A., Supekar, N.T., Gleminich, A.S., and Azadi, P. (2020). Deducing the N- and O-glycosylation profile of the spike protein of novel coronavirus SARS-CoV-2. Glycobiology *30*, 981–988. https://doi.org/10.1093/glycob/cwaa042.

Simmons, G., Reeves, J.D., Rennekamp, A.J., Amberg, S.M., Piefer, A.J., and Bates, P. (2004). Characterization of severe acute respiratory syndrome-associated coronavirus (SARS-CoV) spike glycoprotein-mediated viral entry. Proc. Nat. Acad. Sci. U S A. *101*, 4240–4245. https://doi.org/10.1073/pnas.0306446101.

Stravalaci, M., Pagani, I., Paraboschi, E.M., Pedotti, M., Doni, A., Scavello, F., Mapelli, S.N., Sironi, M., Perucchini, C., Varani, L., et al. (2022). Recognition and inhibition of SARS-CoV-2 by humoral innate immunity pattern recognition molecules. Nat. Immunol. *23*, 275–286. https://doi.org/10.1038/s41590.021-01114-w.

Sztain, T., Ahn, S.-H., Bogetti, A.T., Casalino, L., Goldsmith, J.A., Seitz, E., McCool, R.S., Kearns, F.L., Acosta-Reyes, F., Maji, S., et al. (2021). A glycan gate controls opening of the SARS-CoV-2 spike protein. Nat. Chem. *13*, 963–968. https://doi.org/10.1038/s41557-021-00758-3.

Thompson, A.J., de Vries, R.P., and Paulson, J.C. (2019). Virus recognition of glycan receptors. Curr. Opin. Virol. *34*, 117–129. https://doi.org/10.1016/j.coviro.2019.01.004.

Tian, W., Li, D., Zhang, N., Bai, G., Yuan, K., Xiao, H., Gao, F., Chen, Y., Wong, C.C.L., and Gao, G.F. (2021). O-glycosylation pattern of the SARS-CoV-2

spike protein reveals an "O-follow-N" rule. Cell Res. *31*, 1123–1125. https://doi.org/10.1038/s41422-021-00545-2.

Tortorici, M.A., and Veesler, D. (2019). Structural insight into coronavirus entry. Adv. Virus. Res. *16*, 93–116.

Walls, A.C., Park, Y.-J., Tortorici, M.A., Wall, A., McGuire, A.T., and Veesler, D. (2020). Structure, function and antigenicity of the SARS-CoV-2 spike glycoprotein. Cell *180*, 281–292.

Walls, A.C., Xiong, X., Park, Y.-J., Tortorici, M.A., Snijder, J., Quispe, J., Cameroni, E., Gopal, R., Dai, M., Lanzavecchia, A., et al. (2019). Unexpected receptor functional mimicry elucidates activation of coronavirus fusion. Cell *176*, 1026–1039. https://doi.org/10.1016/j.cell.2018.12.028.

Wang, M.Y., Zhao, M., Gao, L.-J., Gao, X.-F., Wang, D.-P., and Cao, J.-M. (2020). SARS-CoV-2: structure, biology, and structure-based therapeutic development. Front. Cell. Infect. Microbiol. *10*, 587269.

Watanabe, Y., Allen, J.D., Wrapp, D., McLellan, J.S., and Crispin, M. (2020). Site-specific glycan analysis of the SARS-CoV-2 spike. Science *369*, 330–333. https://doi.org/10.1126/science.abb9983.

Zhao, J., Yuan, Q., Wang, H., Liu, W., Liao, X., Su, Y., Wang, X., Yuan, J., Li, T., Li, J., et al. (2020a). Antibody response to SARS-CoV-2 patients with novel coronavirus disease 2019. Clin. Infect. Dis. *71*, 2027–2034. https://doi.org/10.1093/cid/ciaa344.

Zhao, P., Praissman, J.L., Grant, O.C., Cai, Y., Xiao, T., Rosenbalm, K.E., Aoki, K., Kellman, B.P., Bridger, R., Barouch, D.H., et al. (2020b). Virus-Receptor interactions of glycosylated SARS-CoV-2 Spike and human ACE2 receptor. Cell Host Microbe. *28*, 586–601. https://doi.org/10.1016/j.chom.2020.08.004.

Zhu, X., Mannar, D., Srivastava, S.S., Berezuk, A.M., Demers, J.-P., Saville, J.W., Leopold, K., Li, W., Dimitrov, D.S., Tuttle, K.S., et al. (2021). Cryo-electron microscopy structures of the N501Y SARS-CoV-2 spike protein in complex with ACE2 and 2 potent neutralizing antibodies. PLoS Biol. *19*, e3001237. https://doi.org/10.1371/journal.pbio.3001237.

STAR★METHODS

KEY RESOURCES TABLE

REAGENT or RESOURCE	SOURCE	IDENTIFIER
Antibodies		
Anti-hAce2	R&D system	AF933 RRID:AB_355722
SARS-CoV-2 (2019-nCoV) Spike RBD Antibody	Sino Biological	40592_T62
Bacterial and virus strains		
SARS-CoV-2/human/ITA/Milan-UNIMI-1/2020	Laboratory of Serena Delbue	GenBank: MT748758.1
Chemicals, peptides, and recombinant proteins		
GGA328	This paper	Francesconi et al. (2015)
IDS060	This paper	Francesconi et al. (2015)
OFR626	This paper	Francesconi et al. (2015)
OFR622	This paper	Francesconi et al. (2015)
OFR971	This paper	Francesconi et al. (2015)
HisTrap™ High Performance	Sigma	GE17-5247-01
HiPrep™ 26/10 Desalting	Sigma	GE17-5087-01
Critical commercial assays		
CellTiter-Blue ™ cell viability System	Promega	G8080
Bright-Glo™ Luciferase System	Promega	E2610
RNAeasy Kit	Qiagen	74104
2019-nCoV RUO	Integrated DNA Technologies	10006713
Expi293™ Expression System Kit	Gibco™	A14635
Alexa Fluor™ 647 Protein Labeling Kit	Invitrogen™	A20173
Experimental models: Cell lines		
HEK293TN-hACE2	This paper	Original HEK293TN from System Bioscience RRID:CVCL_UL49
Huh7.5	Laboratory of Charles M. Rice	RRID:CVCL7927
Calu3	Laboratory of Anna Kajaste	RRID:CVCL_0609
Expi293 cells	Thermo Fisher Scientific	N/A
Recombinant DNA		
pLenti CMV V5-LUC Blast	Addgene	RRID:Addgene_21474
pMDLg/pRRE (Addgene #12251)	Addgene	RRID:Addgene_12251
pRSV-Rev (Addgene #12253)	Addgene	RRID:Addgene_12253
pcDNA3.1_ spike_del19	Addgene	RRID:Addgene_155297
Plasmid: pcDNA 3.4		
SARS-CoV-2 (2019-nCoV) Spike RBD-His; Gene Bank MN908947	Genscript	Notabartolo et al., 2021
SARS-CoV-2 (2019-nCoV) Spike RBD-His, Gene Bank: B.1.351	Genscript	In this manuscript
SARS-CoV-2 (2019-nCoV) Spike RBD-His, Gene Bank: P1	Genscript	In this manuscript
Software and algorithms		
Prism software	Graphpad	V 9.1.1
FlowJo v10	BD Biosciences	BD Biosciences
UNICORN 7.1	GE Healthcare/Cytiva	GE Healthcare

RESOURCE AVAILABILITY

Lead contact

Further information and requests for resources and reagents should be directed to and will be fulfilled by the lead contact, Cristina Nativi (cristina.nativi@unifi.it).

Materials availability

Plasmids generated have been deposited to Addgene (pLENTI_hACE2_HygR code #155296, pcDNA3.1_spike_del19 code #155297)

Data and code availability

The data reported in this paper will be shared by the lead contact Cristina Nativi (cristina.nativi@unifi.it) upon request. This paper does not report original code. Any additional information required to reanalyze the data reported in this paper is available from the lead contact upon request

EXPERIMENTAL MODEL AND SUBJECT DETAILS

Cells

HEK293TN-hACE2 cells, in house generated, were maintained in DMEM, supplemented with 10% FBS, 1% glutamine, 1% penicillin/streptomycin and 250 μg/mL Hygromycin (GIBCO). Huh-7.5 (RRID:CVCL7927) cells were cultured in DMEM medium supplemented with 10% FBS, 1% glutamine and 1% penicillin/streptomycin. Calu3 cells were cultured in DMEM medium supplemented with 10% FBS, 1% glutamine and 1% penicillin/streptomycin.

Plasmids

pMD2.G/VSV-G (Addgene #12259), pRSV-Rev (Addgene #12253), pMDLg/pRRE (Addgene #12251), pcDNA3.1-hACE2 (Addgene #145033) pcDNA3.1-SARS2-Spike (# 145032), pLenti CMV V5-LUC Blast (Addgene #21474).

Viral strain

Severe acute respiratory syndrome coronavirus 2 isolate SARS-CoV-2/human/ITA/Milan-UNIMI-1/2020, GenBank: MT748758.1.

METHODS DETAILS

HEK293TN-hACE2 generation

HEK293TN-hACE2 were generated by lentiviral engineering of HEK293TN (obtained from System Bioscience) to stably express hACE2 receptor. Lentiviral vectors were produced following a standard procedure based on calcium phosphate cotrasfection with 3rd generation helper and transfer plasmids. The following helper vectors were gifts from Didier Trono: pMD2.G/VSV-G (Addgene #12259), pRSV-Rev (Addgene #12253), pMDLg/pRRE (Addgene #12251). The transfer vector pLENTI_hACE2_HygR was obtained by cloning of hACE2 from pcDNA3.1-hACE2 (a gift from Fang Li, Addgene #145033) into pLenti-CMV-GFP-Hygro (a gift from Eric Campeau & Paul Kaufman, Addgene #17446). hACE2 was amplified by PCR and inserted under the CMV promoter of the pLenti-CMV-GFP-Hygro after GFP excision with XbaI and SalI digestion. pLENTI_hACE2_HygR is now available to the scientific community through Addgene (Addgene #155296). The hACE2 lentiviral vectors thus obtained were used to transduce HEK293TN. 48h after transduction cells were subjected to antibiotic selection with hygromycin at 250 μg/mL. Expression of hACE2 in transduced cells was confirmed by flow cytometry staining using Anti-hAce2 (AF933, R&D system) primary antibody (0.75 μg/200.000 cells) and rabbit anti-goat IgG (Alexa Fluor 647) secondary antibody (1:200 in PBS +2% FBS). The expression of hACE2 was observed in more than 90% of the cells and found to be stable after several passages.

SARS-CoV-2 pseudotype particles generation

To generate SARS-CoV-2 lentiviral pseudotype particles, 5 × 10^6 HEK-293TN cells were plated in 15-cm dishes with complete DMEM medium. The following day, 32 μg of reporter plasmid pLenti CMV V5-LUC Blast (Addgene #21474), 12.5 μg of pMDLg/pRRE (Addgene #12251), 6.25 μg of pRSV-Rev (Addgene #12253), and 9 μg pcDNA3.1_ spike_del19 were co-transfected following a standard procedure based on calcium phosphate transfection. pcDNA3.1_ spike_del19 was generated by deletion of last 19 aa of

spike starting from pcDNA3.1-SARS2-Spike (a gift from Fang Li, Addgene plasmid # 145032) and is now available through Addgene (Addgene #155297). After 12h from transfection medium was changed with 16 ml complete ISCOVE for each dish. At 30 h after transfection, the supernatant was collected, clarified by filtration with a 0.45-μm pore-size filter and concentrated 400× by centrifugation 2h at 20,000 rpm using SW32Ti. Viral pseudoparticles were aliquoted and stored at −80°C.

Single point mutation in pcDNA3.1_ spike_del19 were generated using QuikChange II Site-Directed Mutagenesis Kit.

Spike variants α, β, γ, δ and o were obtained from pcDNA3.1_ spike_del19 by GeneScript mutagenesis service.

Neutralization assays

For lentiviral pseudotype neutralization assay, HEK293TN-hACE2 were plated at 10^4 cells/well in white 96-well plates in complete DMEM medium. The day after cells were infected with indicated MOI of SARS-CoV-2/luciferase pseudoparticles that were subjected to preincubation with biomimetic lectins for 1h at 37°C. For the primary screening, biomimetic lectins were first tested in triplicates at concentrations of 10 μM or 1μM, as indicated. For dose-response tests of selected biomimetic lectins, a 7-point dose-response curve plus untreated control was obtained using 1:2 serial dilutions, starting from 50 μM.

In more detail, biomimetic lectins were diluted in the indicated buffer to 200× final concentration. Each dilution was incubated for 1 h at 37°C with 200 μL of culture medium containing the number of infectious units of SARS-CoV-2 pseudoparticles necessary to obtain the indicated MOI. For example, 10^3 infectious units/50 μL were used to obtain 0.1 MOI of infection. The number of infectious units is previously calculated through FACS titration of SARS-CoV-2/GFP pseudoparticles. After incubation, biomimetic lectins/SARS-CoV-2 pseudoparticles mixture was added to cell at 50 μL/well and plates were incubated for 24h at 37°C. Each dilution was assayed in triplicate. After 24h of incubation pseudoparticle cell infection was measured by luciferase assay using Bright-Glo™ Luciferase System (Promega) while cell viability was measured by fluorescence assay using CellTiter-Blue™ cell viability System (Promega). Infinite F200 plate reader (Tecan) was used to read luminescence and fluorescence signal. Obtained RLUs were normalized to controls and dose response curve were generated by nonlinear regression curve fitting to calculate IC_{50} (GraphPad Prism). For evaluating the inhibition of CBAs by binding to the receptor hACE2, HuH7.5 were plated at 10^4 cells/well in white 96 well plates in complete DMEM medium. After one day, cells were preincubated with biomimetic lectins 1h at 37°C and the infected with indicated MOI of SARS-CoV-2/luciferase pseudoparticles. After 24h of incubation pseudoparticle cell infection was measured as described above.

Cloning, expression, and purification of recombinant SARS-CoV-2 proteins

Human codon-optimized nucleotide sequences encoding RBD (aa 318–541) based on an early SARS-CoV-2 sequence isolate (Wuhan-Hu-1; GenBank: MN908947) and variants B.1.1.7, B.1.351 and P1, were purchased from Genscript and subcloned into the pcDNA3.4 mammalian expression vector, along with a custom N-terminal signal peptide optimized for protein secretion and fused to a C-terminal octa-histidine tag for purification. The resulting plasmid (30 μg) was used to transiently transfect Expi293 cells (approximately 75 × 10^6 cells/mL in a 30 ml culture, at viability >95%) (Expi293™ Expression System, Thermo Fisher Scientific), using the ExpiFectamine293 Reagent, following the manufacturer's recommendation and cultured for 3 days at 37°C in humidified atmosphere of 8% CO2 in air on an orbital shaker. Recombinant RBD was purified from cell culture supernatant using Ni_2^+-NTA affinity chromatography (ÄKTATM Pure, GE Healthcare Life Sciences). Cell supernatants were clarified by centrifugation and buffer was exchanged with binding buffer (Tris 20 mM, NaCl 10 mM, imidazole 10 mM pH 8) using a HiPrep™ 26/10 desalting column. Supernatants were loaded onto a Ni_2^+-NTA column pre-equilibrated with binding buffer. The resin was washed with buffer containing 30 mM imidazole and eluted with the same buffer containing 300 mM imidazole at pH 8. Peak fractions were analyzed by SDS-PAGE and those corresponding to soluble proteins were pooled, buffer exchanged using a HiPrep™ 26/10 desalting column running in 1× PBS and stored at 4°C (Figure S1).

Competitive binding assay

The assay measures the ability of the synthetic receptors to interfere with the binding between RBD viral protein and h-ACE2 receptor, present in the HuH7.5 cell line. Purified recombinant RBD proteins from Spike wild type, Spike variants B.1.1.7, B.1.351 and P1 was labelled with Alexa Fluor 647 (Life Technologies) and was incubated at the concentration of 6.25 μg/mL on the HuH7.5 cells (seeded in 96 well plate; 10000 cells/well) with different concentrations of IDS060 (0–10μM) or other indicated soluble receptors for 1 h at 37 °C. Unbound protein was removed by washing twice with PBS, and RBD binding was assessed by flow cytometry analysis with the FACSCanto-II (BD Biosciences). Data were analyzed using FlowJo software version 10 (BD Biosciences). The binding inhibition was referred to HuH7.5 cells incubated with RBD only, considered as 100% of binding.

NMR spectroscopy

The saturation transfer difference (STD) spectra were recorded at 298 K on a Bruker Avance NEO NMR spectrometer operating at 950 MHz 1H Larmor frequency, equipped with a cryogenically cooled probe. All spectra were processed with the Bruker TOPSPIN software packages. The saturation transfer difference (STD) experiments were acquired with a pseudo-2D pulse sequence and 512 scans on a solution containing a Spike RBD to ID060 molar ratio of 1:40. Saturation was achieved with a cascade of Gaussian pulses of 50 ms duration that were applied for 2.5 s. Selective saturation of the Spike RBD was achieved by applying the on-resonance irradiation at −2 ppm, near to protein signals but far from those of the ligand IDS060. The off-resonance irradiations were applied at −40 ppm.

Propagation of SARS-CoV-2 and *in vitro* infection

Severe acute respiratory syndrome coronavirus 2 isolate SARS-CoV-2/human/ITA/Milan-UNIMI-1/2020, GenBank: MT748758.1 was propagated onto VERO-E6 cells. Briefly, 4 x 10^5 VERO-E6 cells were plated into 6-well plates in DMEM 2% FBS. 24 h later cells were inoculated with 0.01 MOI of the original SARS-CoV2 stock (a kind gift of Professor Serena Delbue, UNIMI). SARS-CoV2 was collected 48–72 h later, filtered through a PES 0.45 μm filter, aliquoted and stored at −80°C. SARS-CoV2 infection in the presence of biomimetic lectins was carried on the non-small-cell lung cancer cell line Calu3. Briefly, 80.000 cells were seeded in 48-well plate in complete DMEM. 24 h later, SARS-CoV2 dilutions to obtain MOI = 1 or MOI = 0.1 were pre-incubated with the indicated concentrations of biomimetic lectins for 30 min at 37°C Calu3 were then infected with the SARS-CoV2/biomimetic lectins. One day post infection cellular RNA was isolated using RNAeasy Kit (Qiagen) and expression of NP was determined by Taqman PCR (2019-nCoV RUO Integrated DNA Technologies).

QUANTIFICATION AND STATISTICAL ANALYSIS

Data are expressed as mean ± SD of two or three replicates, as indicated in figure legends, and represented using Graphpad Prism. Dose-response curve and IC_{50} values are generated by non-linear regression four parameters fitting curves using Graphpad Prism.